ADVANCED THERAPEUTICS
www.advtherap.com

Targeting of Immune Cells with Trimannosylated Liposomes

Karolin Wagener, Matthias Bros, Matthias Krumb, Jens Langhanki, Stefanie Pektor, Matthias Worm, Meike Schinnerer, Evelyn Montermann, Matthias Miederer, Holger Frey, Till Opatz, and Frank Rösch*

Dendritic cells (DCs) are a compelling target in cancer immunotherapy as they initialize strong antigen-specific immune responses. Drug delivery systems (DDSs) such as liposomes provide the opportunity to deliver antigens and immunostimulatory molecules to DCs, which in turn initiate an antigen-specific immune response. To address predominantly DCs, DDSs need to be equipped with targeting moieties. This study evaluates liposomes, bearing the oligosaccharide trimannose on their surface, for their ability to address DCs in vitro and in vivo. Trimannose as a saccharidic structure is known to be recognized by receptors on the surface of DCs. To obtain trimannosylated liposomes, azide-bearing trimannose is coupled to alkyne-functionalized hyperbranched polyglycerol (*hb*PG) with a bis(hexadecyl)glycerol (BisHD) anchor in a Cu(I)-catalyzed alkyne-azide cycloaddition (CuAAC). To enable tracking of the liposomes in vivo, the trimannosylated BisHD-*hb*PG lipids are radiolabeled with ^{18}F in a CuAAC. Subsequently, liposomes are produced via the thin-film hydration method followed by extrusion. The behavior of the trimannosylated liposomes is evaluated in in vitro cell binding assays and in vivo μPET and ex vivo biodistribution studies in healthy C57BL/6 mice and the results are compared to similar liposomes not bearing trimannose on their surface.

1. Introduction

Dendritic cells (DCs) are antigen-presenting cells which are capable to initiate and shape an immune response upon stimulation.[1] DCs are present in most tissues, with an increased abundance at body surfaces such as skin and internal or mucosal membranes, such as the respiratory and gastrointestinal tract.[2] Immature DCs are extremely efficient in capturing antigens. Exogenous pathogens are taken up via micropinocytosis, receptor-mediated endocytosis, and phagocytosis, which initialize DC activation. In an early phase of DC activation, the antigen uptake capacity is enhanced, followed by downregulation. Subsequently, the surface expression of antigen-loaded major histocompatibility complexes (MHCs) and costimulatory receptors is upregulated. At the same time, the DCs migrate to draining lymphoid organs. Upon arrival, the DCs sequentially contact numerous T cells. Due to the presence of costimulatory molecules on the DC surface, antigen-specific T cells are activated. Fully activated $CD8^+$ T cells, termed cytotoxic T lymphocytes, are able to recognize and kill infected and malignant cells displaying the same antigenic peptide via MHCI.[3] In contrast, activated cluster of differentiation 4^+ ($CD4^+$) T cells which recognize antigens in the context of MHCII, polarize toward different so-called T helper cell populations, which contribute to both $CD8^+$ T cell and B-cell activation.[4] In this way, both a cellular and humoral adaptive immune response are initiated.

Dr. K. Wagener, Prof. F. Rösch
Institute of Nuclear Chemistry
Johannes Gutenberg University
Fritz-Strassmann-Weg 2, Mainz 55128, Germany
Dr. M. Bros, E. Montermann
Department of Dermatology
University Medical Center
Langenbeckstraße 1, Mainz 55101, Germany
The ORCID identification number(s) for the author(s) of this article can be found under https://doi.org/10.1002/adtp.201900185

DOI: 10.1002/adtp.201900185

M. Krumb, Dr. J. Langhanki, Dr. M. Worm, Dr. M. Schinnerer, Prof. H. Frey, Prof. T. Opatz
Department of Chemistry
Johannes Gutenberg University
Duesbergweg 10–14, Mainz 55128, Germany
E-mail: krumb@uni-mainz.de
Dr. S. Pektor, Dr. M. Miederer
Clinic and Polyclinic of Nuclear Medicine
University Medical Center
Langenbeckstraße 1, Mainz 55101, Germany
Dr. M. Schinnerer
Institute of Physical Chemistry
Johannes Gutenberg University
Jakob-Welder-Weg 11, Mainz 55128, Germany

The unique ability of DCs to stimulate even naive T cells makes them a very interesting target for an active cancer immunotherapy, which aims to destroy tumor cells exploiting the immune system. To this end, administration of tumor-specific antigens plus adjuvants to DCs is intended to induce a tumor-specific immune response, which aims to destroy both the primary tumor and metastases. To date, this approach remains challenging, as its success not only depends on the effective delivery of carefully selected tumor antigens, but also needs to overcome several mechanisms that mediate immune tolerance.[5] An initial step that may result in a suboptimal immune response is insufficient activation of DCs, caused by a poor (co)delivery of adjuvants. Furthermore, the amount of antigens delivered might be too low, to result in a proper immune response.

Drug delivery systems (DDSs) have the potential to overcome these problems, since large numbers of antigens and activating molecules can be effectively transported and codelivered by these systems. In view of cancer immunotherapy, trifunctional ferrous nanoparticles have been used to address DCs to inhibit growth of established melanoma as a model system in our previous work.[6] With regard to clinical implementation however, one of the most successful types of DDSs are liposomes.[7] These spherical vesicles are biodegradable, demonstrate an excellent biocompatibility, and exhibit a low toxicity, since phospholipids as their main component are also the building blocks of cellular membranes.[8] The linkage of hydrophilic polymers to these phospholipids results in liposomes with a shielding polymer shell on their surface. These so-called stealth liposomes show a prolonged retention in the blood as the polymer shell prevents detection by the mononuclear phagocytic system (MPS) via steric repulsion.[9]

However, in order to deliver antigens as well as adjuvants, suitable targeting moieties are required to address DCs. These components can be coupled to the surface of DDSs. Saccharidic structures, especially mannose-rich structures, are promising targeting vectors as they are recognized by receptors on the surface of DCs and other antigen-presenting cell types.[10] To date, several of these glycan-binding receptors are known, among them the macrophage mannose receptor, which is predominantly expressed by macrophages, whereas dectin-1, DC-specific ICAM-3 grabbing nonintegrin (DC-SIGN), and langerin are predominantly expressed by DCs.[11] Although each receptor type binds mannose-containing structures, their individual morphology causes specific recognition profiles for different structures. The macrophage mannose receptor for instance is rather adapted for the recognition of end-standing single mannose units or a dimannoside cluster, whereas the tetrameric DC-SIGN, which is highly expressed on DCs and only very restrictedly on macrophages,[12] has a higher affinity for branched mannoside structures with a short spacing between the residues.[13] Mitchell and coworkers showed that the branched mannose (Man)-rich oligosaccharide $Man_9GlcNAc_2$ binds 130-fold more tightly to DC-SIGN than mannose, while the overall binding affinity was found to be in the millimolar range.[14] Crystal structures of carbohydrate-recognition domains of DC-SIGN bound to oligosaccharides revealed that the trimannose core structure Manα1-3[Manα1-6]Manα (which is present twice in the aforementioned $Man_9GlcNAc_2$) is important for binding.[15] Furthermore, Feinberg et al. suggested that multiple modes of binding enhance the affinity for DC-SIGN.[16] In fact, liposomes coated with multiple trimannose molecules on their surface gave promising results in cell studies on human monocyte-derived DCs.[17]

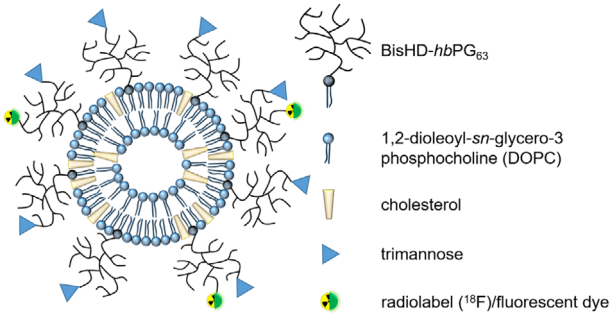

Figure 1. Illustration of a two-dimensional cross-section of the formulated liposome. The liposome consists of BisHD-*hb*P_{63}, DOPC, and cholesterol. The corresponding liposome components are described on the right hand side. The polymeric chains of BisHD-*hb*PG_{63} are functionalized with fluorescent (OG488) as well as radioactive (^{18}F) labels. Both sides of the liposome are equally composed, while, the polymer chains at inside the liposome are omitted for clarity. The illustration is not drawn to scale.

Thus, we aimed to investigate the potential of stealth liposomes, bearing multiple molecules of the aforementioned trimannose core structure Manα1-3[Manα1-6]Manα on their surface, to address DCs in vivo. The shielding polymer shell of the liposomes consisted of the highly biocompatible and water-soluble hyperbranched polyglycerol (*hb*PG),[18] the anchorage of which in the lipid bilayer was provided by an 1,2-bis(hexadecyl)glycerol (BisHD) anchor. This multifunctional polyether lipid has recently been investigated by our group and featured a stable anchorage in the lipid bilayer, while corresponding liposomes exhibited a favorable biodistribution with a prolonged circulation in the bloodstream.[19] To obtain trimannosylated liposomes, (1-(2-(2-(2-(2-azidoethoxy)ethoxy)ethoxy)ethyl)-1*H*-1,2,3-triazole-4-yl)methoxy)-3,6-di-*O*-α-D-mannopyranosyl-α-D-mannopyranoside (trimannose azide) was reacted with alkyne$_4$-BisHD-*hb*PG_{63} in a copper-catalyzed alkyne-azide cycloaddition reaction (CuAAC). To track the liposomes in vitro, the trimannosylated polyether lipids were labeled with the fluorescent dye Oregon Green (OG)488, whereas for in vivo experiments, trimannose-alkyne-BisHD-*hb*PG_{63} was radiolabeled with the prosthetic group 1-azido-2-(2-(2-[^{18}F]fluoroethoxy)ethoxy)ethane ([^{18}F]F-TEG-N_3) via CuAAC, resulting in an [^{18}F]F-TEG-triazole ([^{18}F]FTT) group. Similar, nonmannosylated polyether lipids were also labeled with Oregon Green 488 and fluorine-18 in order to enable comparison. Subsequently, liposomes were prepared via thin-film hydration followed by automated extrusion. **Figure 1** depicts trimannosylated liposomes labeled with the fluorescent dye OG488 and the radio label ^{18}F, respectively. In vitro evaluation of cellular binding properties of the different polyether lipids and their corresponding liposomal formulations was performed using HEK293 cells transfected with a DC-SIGN expression vector, murine bone marrow (BM) derived DCs, and splenic immune cells by fluorescence-activated cell sorting (FACS). Finally, small animal PET and ex vivo organ distribution studies were performed in order to investigate the in vivo fate of both polyether lipids and the respective liposomal formulations.

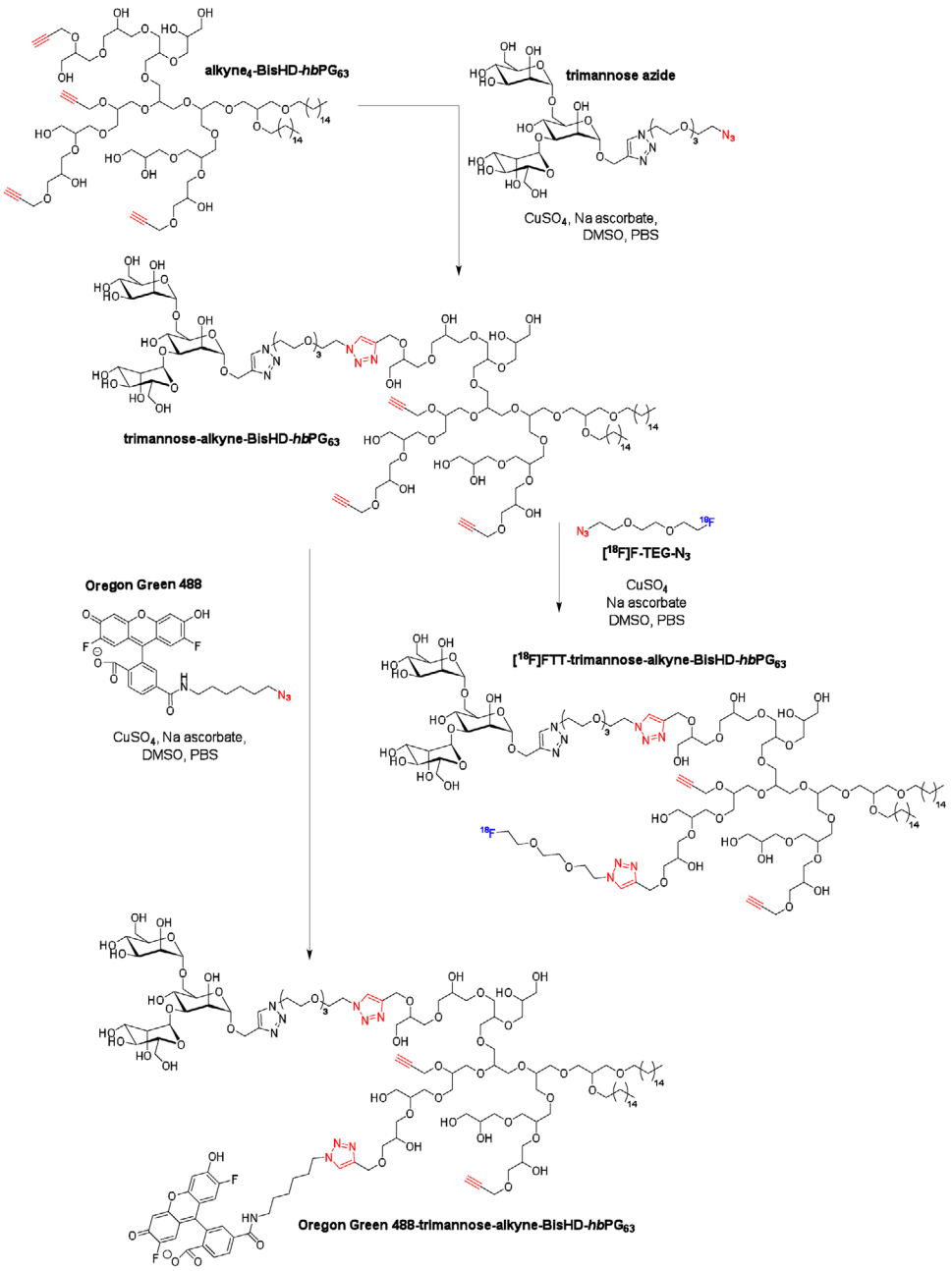

Scheme 1. Synthesis route of [^{18}F]FTT-trimannose-alkyne-BisHD-*hb*PG$_{63}$ and OG 488-trimannose-alkyne-BisHD-*hb*PG$_{63}$. Alkyne$_4$-BisHD-*hb*PG$_{63}$ without trimannose-label was radio- and fluorescence-labeled in the same manner.

2. Results and Discussion

2.1. Organic and Radiosyntheses

In a previous study, we aimed to elucidate the in vivo behavior of liposomes shielded by dialkyl-based polyether lipids.[19] As a main result of this work, it emerged that the liposomes stay intact and circulate in the blood over the investigated period of 4 h. Thus, it was evident to apply a targeting vector, namely the aforementioned trimannose, in order to address DCs. For this purpose, the already evaluated alkyne$_4$-BisHD-*hb*PG$_{63}$[19] appeared to be an ideal choice, since it exhibited on average four alkyne functionalities, allowing for simultaneous linkage of both trimannose and of a radiolabel to track the system in vivo. To this end, we synthesized [^{18}F]FTT-trimannose-alkyne-BisHD-*hb*PG$_{63}$ following the synthesis routes illustrated in **Scheme 1**. For cell studies, trimannose-alkyne-BisHD-*hb*PG$_{63}$, labeled with the fluorescent dye OG 488, was synthesized as well. In the first step, alkyne$_4$-BisHD-*hb*PG$_{63}$ was functionalized with trimannose azide in a CuAAC. The usage of two equivalents of trimannose azide resulted in a degree of functionalization of 1.5 as revealed by diffusion-ordered NMR spectroscopy (Figure S1, Supporting

Information). Due to the difference in size between trimmanose azide and alkyne$_4$-BisHD *hb*PG$_{63}$, purification via spin filtration was straightforward and time-efficient. Subsequently, functionalization with OG 488 was accomplished via CuAAC as well. In contrast to functionalization with trimmanose, which required only small amounts of DMSO, the reaction had to be carried out in a 1:1 mixture of water–DMSO due to the poor solubility of OG 488 in an aqueous environment. Dialysis of the reaction mixture against water enabled the removal of DMSO, which would have damaged the subsequently used spin filter. Since the lipophilic fluorescent dye forms micelles with the amphiphilic polyether lipids, the spin filtration had to be carried out many times (18×) in order to reach an appropriate separation (UV–Vis spectra of the final concentrate as well as of representative filtrates are provided in Figure S2, Supporting Information).

To enable in vivo tracking of trimannose-alkyne-BisHD-*hb*PG$_{63}$ and respective liposomes, trimannose-alkyne-BisHD-*hb*PG$_{63}$ was radiolabeled with [^{18}F]F-TEG-N$_3$ in a CuAAC. The required [^{18}F]F-TEG-N$_3$ was prepared by nucleophilic fluorination of Ts-TEG-N$_3$ using a semiautomatic custom modular system in yields up to 91%. The synthesis has been described in detail in previous reports.[19,20] The subsequent radiolabeling of trimannose-alkyne-BisHD-*hb*PG$_{63}$ via CuAAC proceeded reliably in radiochemical yields (RCYs) exceeding 95% after 10 min (Figure S3, Supporting Information). Reaction conditions were adopted from the radiolabeling of alkyne$_4$-BisHD-*hb*PG$_{63}$ as specified in a previous report.[19] Radiolabeling and fluorescence labeling of alkyne$_4$-BisHD-*hb*PG$_{63}$ was accomplished in the same manner as for its trimannosylated counterpart (Figures S2 and S3, Supporting Information).

2.2. Liposome Formation and Characterization

Liposomes were prepared by the thin film hydration method followed by repeated extrusion through polycarbonate membranes with pore diameters of 400 nm, 100 nm, and then 50 nm. Extrusion was performed using an automatic extrusion device described in a previous report,[19] which allows for a reproducible pressure during the extrusion process and is regulated by a separate control module. Via this automatization, it was possible to obtain liposomes with reproducible sizes (see below). Furthermore, the separate control module allows for remote control of the extrusion device, and therefore considerably reduces the radiation exposure of the experimentalist. After the extrusion, liposomes were separated from nonintegrated lipids via size exclusion chromatography (SEC) with phosphate-buffered saline (PBS) as the mobile phase. Liposomes eluted in the fractions 3–5.

The size of the liposomes was determined via dynamic light scattering (DLS), when ^{18}F-activity (^{18}F has a half-life of 109.7 min)[21] had ceased (≈18 h). Alkyne$_4$-BisHD-*hb*PG$_{63}$-shielded (5 mol%) liposomes exhibited a hydrodynamic radius R_h of 94 nm, whereas liposomes shielded with trimannose-alkyne-BisHD-*hb*PG$_{63}$ (5 mol%) showed an R_h value of 109 nm (DLS data are provided in Figure S4, Supporting Information). Furthermore, storage stability experiments were conducted, indicating that the liposomes are stable at least over a period of 1 month (Figure S5, Supporting Information).

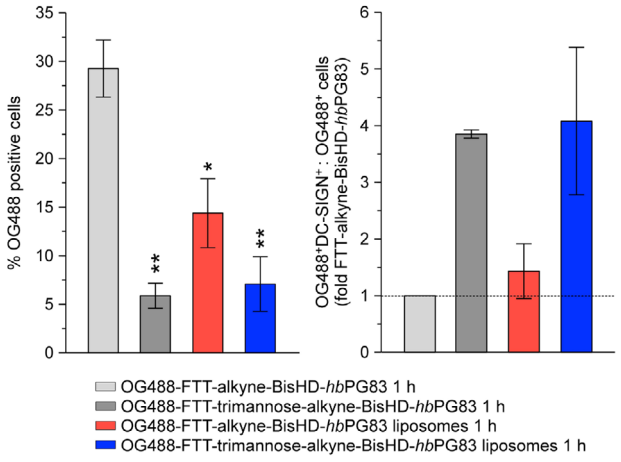

Figure 2. Binding properties of differentially functionalized lipid ether and derived liposomes to HEK293 cells engineered to express DC-SIGN. HEK293 cells were transfected with a DC-SIGN expression vector. On the next day, transfectants were cooled on ice, and incubated with serum-preincubated OG488-labeled formulations for 1 h. The frequencies of OG488-positive cells (left panel) and the ratios of OG488/DC-SIGN double-positive and OG488$^+$ DC-SIGN$^-$ cells (right panel) were assessed by flow cytometry (right panel). In each experiment, the ratios were normalized to the value obtained for treatment with OG488-FTT-alkyne-BisHD-*hb*PG83. Data denote the mean ± SEM ($n = 3$). Statistically significant differences versus OG488-FTT-alkyne-BisHD-*hb*PG83 are indicated. *$p < 0.05$, **$p < 0.01$ (one-way ANOVA, Tukey test). The gating strategy of flow cytometric analysis is depicted in Figure S6, Supporting Information, and results of flow cytometric analysis are shown in Figure S7, Supporting Information.

2.3. In Vitro Studies

2.3.1. Binding Studies Using DC-SIGN Expressing Cells

First, we investigated whether trimannosylated polyether lipids and according liposomes preferentially engaged the DC-SIGN receptor. To this end, HEK293 cells which lack endogenous DC-SIGN expression were transfected with a mouse DC-SIGN expression vector to obtain a subpopulation that expressed this C-type lectin receptor (Figure S33, Supporting Information). To take into account the potential formation of a protein corona around the nanoparticulate formulations in vivo, the different formulations were incubated with native mouse serum prior to application to the cells.

Nonmannosylated polyether lipids displayed the strongest cellular binding of all tested formulations which was reduced by about 80% in case of trimannosylated polyether lipids (**Figure 2**, left panel). Nonmannosylated liposomes displayed an intermediate binding efficiency of almost 15% which was about halved in case of the trimannosylated liposomes. To evaluate DC-SIGN binding specificity of the various formulations, the ratios of OG488$^+$DC-SIGN$^+$ and OG488$^+$DC-SIGN$^-$ cells were calculated. In general, trimannosylated formulations displayed an almost four-fold higher ratio than nonmannosylated lipid ether, and nonmannosylated liposomes showed a similar low binding specificity as the respective lipid ether itself (Figure 2, right panel). These results indicate that trimannosylation reduced overall (unspecific) cellular binding of lipid ether–liposomes and increased specificity of binding to DC-SIGN expressing cells.

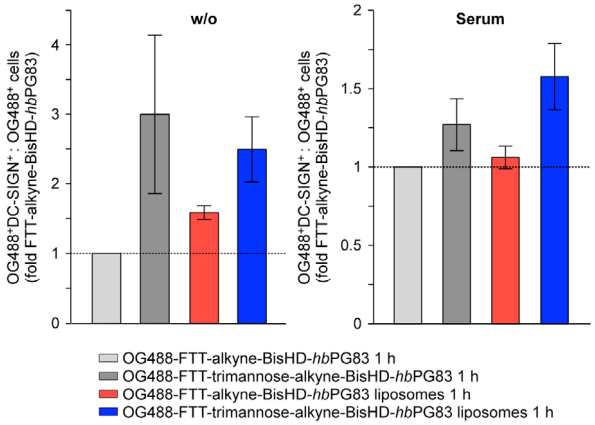

Figure 3. DC binding properties of trimannosylated lipid ether and derived liposomes. The different OG488-labeled formulations were left untreated (w/o) or were preincubated with mouse serum, and were applied to BMDC (37 °C, 1 h). OG488 and DC-SIGN expression of $CD11c^+$ BMDC was assessed by flow cytometry. Graphs show the ratios of $OG488^+$DC-$SIGN^+$ and $OG488^+$DC-$SIGN^-$ BMDC. In each experiment, the ratios were normalized to the value obtained for treatment with OG488-FTT-alkyne-BisHD-*hb*PG83. Data denote the mean ± SEM ($n = 3$). The gating strategy is depicted in Figure S9, Supporting Information, and primary results of one experiment are shown in Figure S10, Supporting Information.

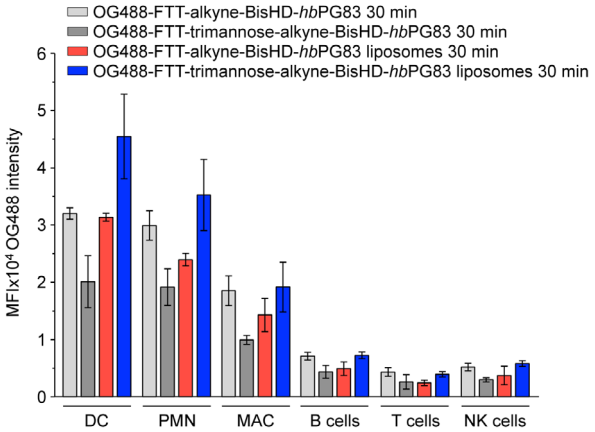

Figure 4. Spleen cell binding of differentially functionalized lipid ether and derived liposomes. Spleen cells were incubated with the different OG488-labeled formulations at 37 °C for 30 min. For each immune cell type, OG488 intensity was assessed by flow cytometry. Data denote the mean ± SD ($n = 2$). The gating strategy is shown in Figure S11, Supporting Information, and representative histograms are presented in Figure S12, Supporting Information.

2.3.2. DC Binding Studies

Next, we asked for the binding specificity of trimannosylated formulations to DC-SIGN expressing DC. For this, we used BM derived DCs, a major subpopulation of which expressed this C-type lectin receptor (Figures S35 and S36, Supporting Information). Nonmannosylated lipid ether engaged $CD11c^+$ BMDC at highest level, largely irrespective of pretreatment with serum (85–90%; Figure S7, Supporting Information). Trimannosylated lipid ether showed moderately reduced BMDC binding. Nonmannosylated and trimannosylated liposomes bound BMDC to a similar extent as the respective lipid ethers, respectively. Similar results were observed when incubating BMDC with the different formulations at 4 °C. These findings are reminiscent to the binding behavior observed in HEK293 cells, although in case of that cell line, overall binding was reduced more strongly in case of incubation with trimannosylated formulations. This difference may be attributed to the strong endocytotic capacity of DCs. Trimannosylated lipid ether bound DC-$SIGN^+$ BMDC at higher level than nonmannoslyated lipid ether, and the corresponding types of derived liposomes showed a similar binding behavior (**Figure 3**, left panel). Interestingly, when using formulations pretreated with serum, the effect of trimannosylation-mediated elevated binding to DC-$SIGN^+$ BMDC was markedly attenuated (Figure 3, right panel). This effect may be explained by enrichment of serum components at the formulations' surface modulating their interaction with DC surface receptors.

2.3.3. Spleen Cell Binding Studies

Besides DCs, other immune cell types including macrophages (MAC) and polymorphonuclear neutrophils (PMN) are specialized in the detection of pathogens by distinct types of danger receptors and have a strong endocytic–phagocytic capacity. With regard to subsequent in vivo studies, we evaluated the immune cell type specific binding properties of serum-preincubated trimannosylated formulations at 37 °C using total murine spleen cells. Splenic DCs and PMNs showed comparable binding of nonmannosylated lipid ether which was moderately diminished in case of trimannosylation (**Figure 4**).

This observation is in accordance with the "shielding" effect of trimannosylation observed for both HEK293 cells and BMDCs. Nonmannosylated liposomes displayed similar (DC) or reduced (PMN) binding intensities as compared with the according lipid ether. Notably, trimannosylated liposomes bound to the highest extent to DCs and at higher levels than any other formulation. PMNs displayed somewhat lower binding of these liposomes. In case of MACs, a similar binding pattern of the different formulations was observed as for PMNs, albeit at lower intensities. B cells, T cells, and NK cells presented negligible binding of either formulation. A similar cell type dependent binding pattern was also observed when performing incubations at 4 °C (not shown). Taken together, these result suggest that trimannosylated liposomes may bind to DCs, most probably in part via DC-SIGN, and to other immune cell types with endocytic potential (PMN, MAC) to a considerably higher extent than lipid ethers as well as nonmannosylated liposomes.

2.4. Animal Studies

2.4.1. In Vivo μPET Studies

To investigate the in vivo fate of the trimannosylated versus the nonmannosylated polyether lipids and their corresponding liposomal formulations, μPET studies were conducted in healthy, male C57BL/6 mice. Dynamic scans of 1 h were started at the time of injection in order to follow the initial distribution. For the liposomal formulations, static scans of 30 min were also run 3.5 h after injection to monitor pharmacokinetics at later

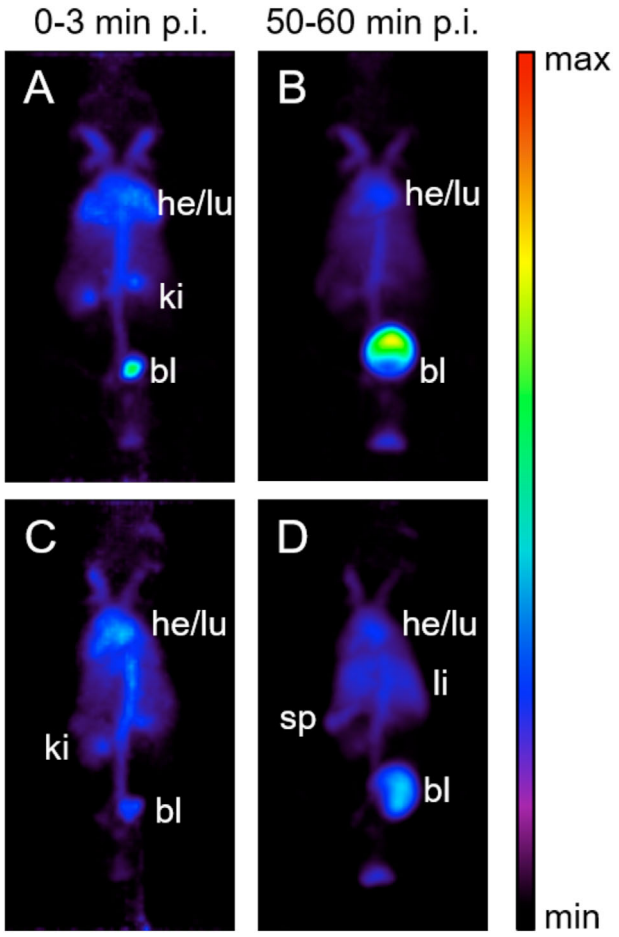

Figure 5. Coronal, whole-body maximum intensity projections (MIPs) of different time frames for [^{18}F]FTT-alkyne-BisHD-*hb*PG$_{63}$ (A,B) and [^{18}F]FTT-trimannose-alkyne-BisHD-*hb*PG$_{63}$ (C,D). he: heart, lu: lung, bl: bladder, ki: kidney, sp: spleen, li: liver.

stages. **Figure 5** shows coronal, whole-body maximum intensity projections (MIPs) of the polyether lipids [^{18}F]FTT-alkyne-BisHD-*hb*PG$_{63}$ and [^{18}F]FTT-trimannose-alkyne-BisHD-*hb*PG$_{63}$. Shortly after injection, both polyether lipids showed an initial uptake in the blood stream (0–3 min) and were subsequently excreted renally. As expected, after 1 h both polyether lipids were mainly localized in the bladder, since the molecular weight of both polyether lipids was below the renal threshold, and the large hydrophilic polyether block prevented hepatobiliary excretion. However, despite the competing renal excretion, small differences in liver and spleen uptake were observed, as [^{18}F]FTT-trimannose-alkyne-BisHD-*hb*PG$_{63}$ exhibited a higher uptake in these organs than the nonmannosylated [^{18}F]FTT-alkyne-BisHD-*hb*PG$_{63}$.

In contrast, the liposomal formulations behave fundamentally differently from the nonassociated polyether lipids. **Figure 6** shows coronal, whole-body MIPs of liposomes shielded by [^{18}F]FTT-alkyne-BisHD-*hb*PG$_{63}$ or by [^{18}F]FTT-trimannose-alkyne-BisHD-*hb*PG$_{63}$ at different times after injection. Both types of liposomes initially (0–3 min) circulated in the bloodstream, which can be deduced from the observation that the activity was largely confined to well-perfused organs, such as heart and lung. Yet, the trimannosylated liposomes also exhibited accumulation in the spleen (Figure 6D), in contrast to nonmannosylated liposomes (Figure 6A). After 60 min, the difference was considerably more pronounced. For the nonmannosylated liposomes, the activity was still mainly found in the bloodstream with some enrichment in the spleen (Figure 6B), which may be attributed to recognition by DCs, PMNs, and MACs that constitute the MPS. After 4 h, the liver and spleen uptake became dominant, but also some accumulation in well-perfused organs such as heart and lung (Figure 6C), revealing that a fraction of the liposomes continuously circulated in the blood.

The biodistribution of the trimannosylated liposomes was completely different. Here, already after 1 h, almost no more circulation in the blood stream was observed, instead besides liver a strong accumulation was apparent in the spleen (Figure 6E). This effect was intensified after 4 h (Figure 6F). We assign the differences in biodistribution directly to the trimannose moieties on the surface of the liposomes, since the investigated liposomal formulations had similar hydrodynamic radii around 100 nm and the trimannose label possessed the same composition. Further details concerning the PET data are provided in Figures S14 and S15, Supporting Information.

2.4.2. Ex Vivo Biodistribution

Ex vivo biodistribution studies were performed in order to gain quantitative conclusions regarding the in vivo accumulation of the ^{18}F-labeled compounds in different organs. **Figure 7** shows the results for the nonmannosylated in comparison to the trimannosylated polyether lipids (underlying data are provided in Table S1, Supporting Information).

As depicted in Figure 7, after 1 h [^{18}F]FTT-alkyne-BisHD-*hb*PG$_{63}$ was mainly found in urine (35.8 ± 14.6% ID per gram of tissue (% ID/g tissue)) and in the blood (29.8 ± 3.9% ID/g tissue), which confirms that it circulated in the bloodstream until it was excreted via the renal pathway. [^{18}F]FTT-trimannose-alkyne-BisHD-*hb*PG$_{63}$ also circulated in the blood (27.6 ± 2.3% ID/g tissue) and was renally excreted (27.2 ± 8.7% ID/g tissue). However, in contrast to its nonmannosylated counterpart, it displayed a significantly higher uptake in liver (24.5 ± 2.9 vs. 12.1 ± 2.3% ID/g tissue, factor 2), spleen (23.7 ± 3.5 versus 5.9 ± 0.4% ID/g tissue, factor 4), and BM (2.2 ± 0.6 vs. 0.4 ± 0.2% ID/g tissue, factor 5.5) after 1 h. These findings reveal that the trimannose structure altered the biodistribution of lipid ethers. Despite competing renal excretion, the trimannosylated polyether lipids accumulated in the spleen. This was not the case for the nonmannosylated polyether lipids. Preferential accumulation of trimannosylated lipid ethers in liver and spleen as compared with the nonmannosylated formulation suggests stronger binding to cells of the MPS located in these organs. These trimannose-dependent differences in overall binding intensity of lipid ethers have not been observed in our in vitro studies using spleen cells.

The results of the ex vivo biodistribution studies of the corresponding liposomal formulations are shown in **Figure 8** (underlying data are provided in Table S1, Supporting Information). In case of nonmannosylated liposomes, a significant amount of the liposomes was located in the blood

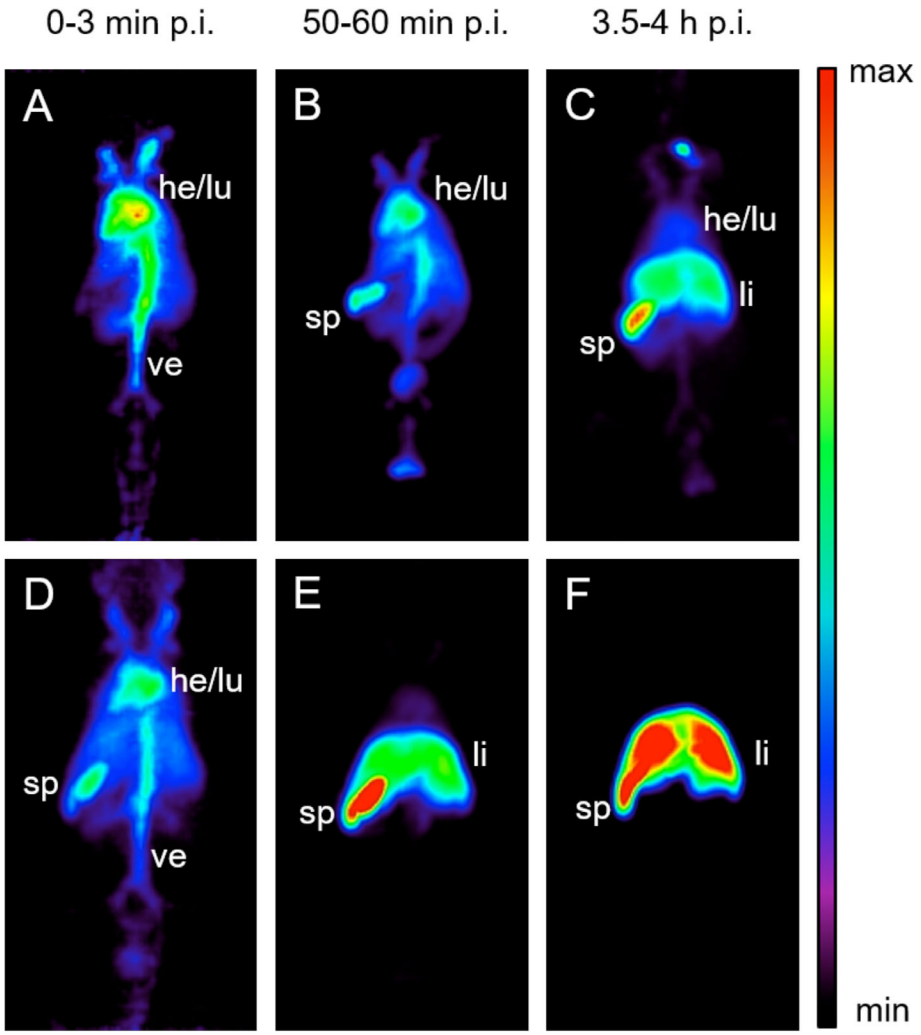

Figure 6. Coronal, whole-body maximum intensity projections (MIPs) at different time points (left column: 0–3 min p.i., middle column: 50–60 min p.i., right column: 3.5–4 h p.i.) for [^{18}F]FTT-alkyne-BisHD-*hb*PG$_{63}$ liposomes (A–C) and for [^{18}F]FTT-trimannose-alkyne-BisHD-*hb*PG$_{63}$ liposomes (D–F). he: heart, lu: lung, ve: vein, sp: spleen, li: liver.

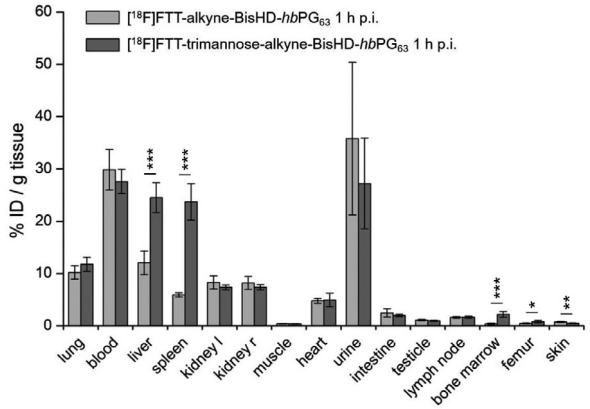

Figure 7. Ex vivo biodistribution data 1 h p.i. of the polyether lipids [^{18}F]FTT-alkyne-BisHD-*hb*PG$_{63}$ and [^{18}F]FTT-trimannose-alkyne-BisHD-*hb*PG$_{63}$ (n=5, each). Statistically significant differences between contents of formulations within a tissue are indicated. $^{*}p < 0.05$, $^{**}p < 0.01$, $^{***}p < 0.001$ (one-way ANOVA, unpaired Student's t-test).

(43.9 ± 2.8% ID/g tissue) 1 h after injection. A major part of the activity can be found in spleen (51.7 ± 4.5% ID/g tissue) and liver (19.6 ± 3.5% ID/g tissue). After 4 h, liver and spleen uptake doubled, whereas levels in the blood halved as compared to the biodistribution 1 h after injection. At 1 h after application, trimannosylated liposomes were almost exclusively present in the spleen (128.7 ± 18.7% ID/g tissue) and in the liver (87.7 ± 20.0% ID/g tissue). This pattern was unaltered when assessed at 4 h after injection. These findings clearly confirm a significant influence of the trimannose on the in vivo fate of the liposomes in correspondence with their preferred binding to DC-SIGN^{+} DC in vitro.

3. Conclusion

In this study, the in vitro binding characteristics and in vivo biodistribution of trimannosylated and similar nonmannosylated polyether lipids and their respective liposomal formulations were

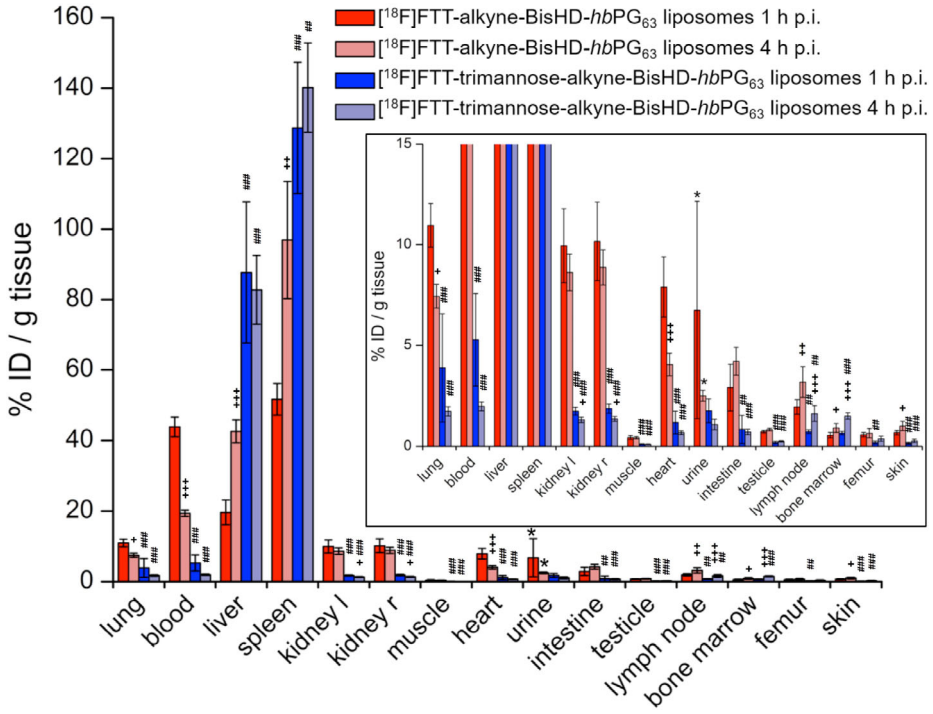

Figure 8. Ex vivo biodistribution data 1 h p.i. and 4 h p.i. of [^{18}F]FTT-alkyne-BisHD-*hb*PG$_{63}$ liposomes and of [^{18}F]FTT-trimannose-alkyne-BisHD-*hb*PG$_{63}$ liposomes ($n = 5$, for each time point and each liposome type). Asterisks indicate $n = 4$. Box: zoomed in on % ID per gram of tissue values below 15. Statistically significant differences between contents of formulations within a tissue are indicated: $^{+}$between same type of formulation at 4 h versus 1 h, $^{\#}$versus [^{18}F]FTT-alkyne-BisHD-*hb*PG83 liposomes at corresponding incubation period (1 h, 4). $^{+,\#}p < 0.05$, $^{++,\#\#}p < 0.01$, $^{+++,\#\#\#}p < 0.001$ (one-way ANOVA, Tukey test). Primary data are presented in Table S1, Supporting Information and are summarized in Figure S16, Supporting Information.

investigated utilizing fluorescence (OG488) labeled derivatives for in vitro cell binding studies, and radioactive labeling with ^{18}F for subsequent in vivo μPET and ex vivo biodistribution studies in mice. It was found that the trimannosylated polyether lipids increasingly accumulated in spleen, liver, and BM, compared to the nonmannosylated polyether lipids. For the liposomal formulations, this effect was even more pronounced. To the best of our knowledge, this is the first report demonstrating the influence of trimannose as active targeting moieties to DCs, both in vitro and in vivo. We tentatively ascribe these differences to a recognition of the trimannose moieties by DCs, which are located particularly in spleen and lymph nodes and also to some extent in the liver. Further, PMN and MAC may contribute to elevated retention of trimannosylated liposomes as well. Altogether, our results are in accordance with earlier cell studies, which revealed that the trimannose structure is bound by human monocyte-derived DCs.[17] Back then, the authors speculated that trimannosylated liposomes engaged the mannose receptor. We show that trimannosylated formulations engage DC-SIGN as expressed by DCs.

4. Experimental Section

Materials: All chemicals were obtained from common chemical suppliers such as Sigma–Aldrich, TCI Europe, VWR, or Acros Organics unless stated otherwise. Oregon Green 488 azide was purchased from Click Chemistry Tools. Deuterated pyridine-d_5 was purchased from Deutero GmbH. Particle-free PBS used for DLS experiments was obtained from Gibco by Thermo Fisher Scientific. Spin filtration was done with Microsep Advance centrifugal filters (molecular weight cut-off: 1 kDa; Pall). Dialysis was accomplished using Spectra/Por 7 dialysis tubing (molecular weight cut-off: 1 kDa, material: regenerated cellulose; Spectrum). [^{18}F]F^-_{aq} was produced by irradiation of enriched [^{18}O]H_2O with protons at a PETtrace 700S cyclotron (GE Healthcare). A common production run lasted 30 min at a beam current of 25 μA, yielding an ^{18}F-activity of 20 GBq.

Characterization: ^{1}H NMR and DOSY spectra of the polymer lipids were measured either on a Bruker Avance III HD 400 MHz (5 mm BBFO SmartProbe and SampleXPress 60 auto sampler) or on a Bruker Avance II 400 MHz (5 mm BBFO probe and SampleXPress 60 auto sampler) at 23 °C. All spectra were processed with MestReNova v11.0 software. DOSY spectra were analyzed using MestReNova Bayesian DOSY Transform. Coupling constants (*J*) are reported in Hertz (Hz) (splitting abbreviations: s, singlet; d, doublet; t, triplet; q, quartet; m, multiplet; br, broad; and combinations thereof).

UV–Vis spectra were acquired on a V-630 UV–Vis spectrophotometer (Jasco), using quartz cuvettes with a layer thickness of 10 mm. Samples of purified polyether lipids were diluted with water (1:1) prior to the measurement. Filtrates of the spin filtration were measured without dilution. Analysis was carried out with Spectra Manager (version 2.04; Jasco).

For multi-angle DLS cylindrical quartz cuvettes (Hellma Analytics, Mühlheim, Germany) were cleaned by dust-free distilled acetone and were transferred to a dust free flow box. Solutions were diluted 1:100 with PBS and filtered into the cuvettes through Millex-LCR filters, 0.45 μm pore size (Merck Millipore). DLS measurements were performed by the following instruments at 20 °C. Apparatus 1 consists of a Uniphase He–Ne Laser (22.5 mW output power at $\lambda = 632.8$ nm) and an ALV/CGS-8F SLS/DLS 5022F goniometer with eight simultaneously working ALV 7004 correlators and eight ALV/High QEAPD avalanche photodiode detectors. Apparatus 2 consists of a Uniphase He–Ne Laser (22.5 mW output power at $\lambda = 632.8$ nm), an ALV/SP125 goniometer with an ALV 5000/E/PCI

correlator and an ALV/High QEAPD Avalanche photodiode detector. The correlation functions of the particles were fitted biexponentially. The z-average diffusion coefficient D_z was calculated by extrapolating D_{app} for $q = 0$. By formal application of Stokes law, the inverse z-average hydrodynamic radius is $R_h = \langle R_h^{-1} \rangle_z^{-1}$. The experimental uncertainties are estimated to ±2% for R_h.

Radio-thin-layer chromatography (radio-TLCs) was run on silica-coated aluminum-backed TLC plates (Merck) using EA–Hex 1:1 as mobile phase. The chromatograms, acquired on a RITA detector (Raytest), were analyzed using Gina Star TLC software (Raytest).

Synthesis of (1-(2-(2-(2-azidoethoxy)ethoxy)ethoxy)ethyl)-1H-1,2,3-triazole-4-yl)methoxy)-3,6-di-O-α-D-mannopyranosyl-α-D-mannopyranoside (trimannose azide): The synthesis protocol was described in previous reports.[22]

Synthesis of alkyne$_4$-1,2-bis(hexadecyl)glycerol-hbPG$_{63}$ (alkyne$_4$-BisHD-hbPG$_{63}$): The synthesis protocol was described in a previous report.[19]

Synthesis of trimannose-alkyne-1,2-bis(hexadecyl)glycerol-hbPG$_{63}$: Alkyne$_4$-BisHD-*hb*PG$_{63}$ (18 mg, 3.4 µmol, 1 eq.) was dissolved in 1 mL of PBS. Subsequently, a solution of trimannose azide (5 mg, 6.7 µmol, 2 eq.) in 1 mL PBS, DMSO (25 µL), $CuSO_4$ (30 µL, 1 M in MilliQ water, 30 µmol), and sodium ascorbate (50 µL 2.4 M in PBS, 120 µmol) was added in this order. The mixture was stirred at room temperature for 12 h under argon atmosphere. Purification was accomplished by spin filtration (30 min, 4696 g). The concentrate was washed 10 times with each 1 mL of MilliQ water, which was added to the concentrate and then centrifuged again (15 min, 4696 g). Lyophilization gave the desired product as a brownish solid (22.5 mg, 1.5× trimannose per BisHD-*hb*PG$_{63}$, calculated from ^{1}H NMR spectroscopy (Figure S1, Supporting Information)). ^{1}H NMR (400 MHz, pyridine-d_5) δ (ppm) = 8.18 (s, br, 3H, $H_{triazole}$, $H'_{triazole}$), 5.91 (s, br, 1.5H, H-1'$_{trimannose}$), 5.60 (s, br, 1.5H, H-1$_{trimannose}$), 5.33 (s, br, 1.5H, H-1''$_{trimannose}$), 4.91–3.30 (m, 359H, all others), 1.74–1.58 (m, 4H, CH_2–CH_2–O_{BisHD}), 1.51–1.36 (m, 4H, CH_2-CH_2-CH_2-O_{BisHD}), 1.36–1.18 (m, 48H, $CH_{2\ BisHD}$), 0.87 (t, 6H, J_{AB} = 6.6 Hz, CH_3–$CH_{2\ BisHD}$).

Synthesis of OG 488-trimannose-alkyne-1,2-bis(hexadecyl)glycerol-hbPG$_{63}$ and OG 488-alkyne-1,2-bis(hexadecyl)glycerol-hbPG$_{63}$: Both compounds were synthesized according to the same procedure. The synthesis of OG 488-alkyne-BisHD-*hb*PG$_{63}$ is described as an example. Alkyne$_4$-BisHD-*hb*PG$_{63}$ (3 mg, 0.6 µmol, 1 eq.) was dissolved in 0.5 µL of PBS. Subsequently, a solution of OG 488 azide (0.5 mg, 0.8 µmol, 1.4 eq.) in 0.5 mL DMSO, $CuSO_4$ (15 µL, 1 M in MilliQ water, 15 µmol), and sodium ascorbate (25 µL, 2.4 M in PBS, 60 µmol) were added in this order. The orange mixture was stirred at room temperature for 12 h protected from light under argon atmosphere. Purification was accomplished by dialysis against water (3 × 600 mL) followed by spin filtration (30 min, 4696 g). The concentrate was washed 10 times with 2 mL of MilliQ–ethanol 9:1, then 8 times with 2 mL MilliQ, which was added to the concentrate and then centrifuged again (15 min, 4696 g). Lyophilization gave the desired product as a brownish solid (2.9 mg). The successful linkage of the fluorescent dye and the separation of unbound dye was determined by UV–Vis spectroscopy. The respective spectra are provided in Figure S3, Supporting Information.

Synthesis of 2-(2-(2-azidoethoxy)ethoxy)ethyl-p-toluenesulfonate (Ts-TEG-N$_3$): The synthesis was accomplished according to a published procedure.[20]

Radiosynthesis of 1-azido-2-(2-(2-[^{18}F]fluoroethoxy)ethoxy)ethane: [^{18}F]F-TEG-N_3 was synthesized on a semiautomatic custom modular system with radiochemical yields (RCY) up to 91% (TLC, EA–nHex 1:1, R_f: 0.8) according to a previous report.[20]

Radiosynthesis of [^{18}F]FTT-trimannose-alkyne-1,2-bis(hexadecyl)glycerol-hbPG$_{63}$ and [^{18}F]FTT-alkyne 1,2-bis(hexadecyl)glycerol-hbPG$_{63}$: The radiolabeling procedure for alkyne$_4$-BisHD-*hb*PG$_{63}$ is described in a previous report.[19] Trimannose-alkyne-BisHD-*hb*PG$_{63}$ was radiolabeled in the same fashion.

Liposome Formation: Liposomes were prepared by the thin film hydration method followed by several extrusion steps. Liposome components were 1,2-dioleoyl-*sn*-glycero-3-phosphocholine (DOPC), cholesterol and fluorescent–radiolabeled BisHD polyether (OG 488-trimannose-alkyne-BisHD-*hb*PG$_{63}$, OG 488-alkyne-BisHD-*hb*PG$_{63}$, [^{18}F]FTT-trimannose-alkyne-BisHD-*hb*PG$_{63}$ or [^{18}F]FTT-alkyne-BisHD-*hb*PG$_{63}$) at molar ratios of 55:40:5 mol%. M_n values, determined by ^{1}H NMR spectroscopy, were used to calculate the lipid compositions. A solution of DOPC in ethanol, cholesterol in ethanol, and the fluorescently labeled–radiolabeled polyether lipid were blended, and the solvent was evaporated in a miniature rotating evaporator to obtain a thin film of the liposome components. 0.8 mL of PBS was added. The liposome suspension was sonicated at 50 °C for 10 min, followed by automated extrusion through polycarbonate membranes with different pore diameters (400 nm, then 100 nm, then 50 nm, 21 times each) using a mini-extruder (AVESTIN Europe GmbH) driven by a custom-built device.[19] Finally, the liposomes were purified via SEC using Sephacryl S-400 HR as a resin (≈4 mL packed in a 6 mL empty SPE tube with 20 µm PTFE frits at top and bottom) and PBS as a mobile phase. Fractions of 0.5 mL were collected. Liposomes eluted in the fractions 3–5.

Cell Studies: The binding properties of OG488-labeled formulations were assessed by flow cytometry. Mouse serum was purified from whole blood derived from C57BL/6 mice by centrifugation using Z Serum Sep columns (Greiner Bio-One, Frickenhausen, Germany). Aliquots of the various OG488-labeled formulations (1 mg mL^{-1} PBS) were preincubated with the same volume of native mouse serum in low protein binding tubes (Greiner Bio-One) at 37 °C for 30 min.

Dependency of cellular DC-SIGN expression for binding of the differentially functionalized formulations was evaluated using HEK293 cells transfected with a DC-SIGN expression plasmid (SourceBioscience, Nottingham, UK). To this end, HEK293 cells were cultured in DMEM supplemented with 5% fetal calf serum (FCS), 2 × 10^{-3} M L-glutamine, 100 U mL^{-1} penicillin, 100 µg mL^{-1} streptomycin (all from Sigma–Aldrich, Deisenhofen, Germany), and 50 × 10^{-6} M β-mercaptoethanol (Roth, Karlsruhe, Germany). For transfection, HEK293 cells were seeded in 12-well cell culture cluster plates (2 × 10^5 mL^{-1}) obtained from Greiner Bio-One. HEK293 cells were transfected at a confluency of 60–70% with DC-SIGN expression construct (2 µg) complexed with JetPEI (Polyplus, Illkirch, France) as recommended by the manufacturer. On the next day, cultures were pre-cooled on ice for 30 min, and serum-preincubated formulations were applied (2 µg of formulation mL^{-1}). After 1 h of incubation, samples were harvested, washed, incubated with a PE-labeled DC-SIGN specific antibody (Thermo Fisher, Waltham, MA), and fixed in FACS buffer containing 0.7% paraformaldehyde. Fixed samples were subjected to flow cytometric analysis using an Attune NxT flow cytometer (Thermo Fisher) equipped with Attune Nxt Software v3.1.1. The gating strategy is shown in Figure S7, Supporting Information.

To associate the cellular binding of the different formulations with the DC-SIGN expression state of DCs, BM-derived DCs were used. For this, BM cells derived from C57BL/6 mice were resuspended in IMDM-based culture medium (supplemented as listed above), containing 10 ng mL^{-1} recombinant murine GM-CSF (R&D Systems, Wiesbaden, Germany) in addition. BM cells were seeded in 12 well suspension cell culture cluster plates (2 × 10^5 mL^{-1}) purchased from Greiner Bio-One. On days 3 and 6 of culture, culture media was replenished. On days 7–8 of culture the differentiated BMDC were incubated in parallel experiments with formulations w/o or preincubated with mouse serum (each 2 µg of formulation mL^{-1}). After 1 h, samples were harvested, washed in staining buffer (PBS containing 2% FCS and 2 × 10^{-3} M EDTA) and incubated with Fcγ blocking antibody (rat anti-mouse CD16/CD32 antibody) for 15 min at 4 °C to prevent unspecific binding of subsequently applied antibodies. Then, samples were incubated with antibodies specific for CD11c (PE/Cy7) and DC-SIGN (PE), fixed and subjected to flow cytometric analysis as outlined above. The gating strategy is presented in Figure S9, Supporting Information.

To monitor binding of the various formulations to primary immune cell populations, spleens were retrieved from C57BL/6 mice using a 40 × 10^{-6} M cell strainer (Greiner Bio-One) to obtain a single cell suspension. Erythrocytes were lysed using a hypotonic lysis buffer. Spleen cells were resuspended in IMDM culture medium (4 × 10^6 mL^{-1}). Spleen cells were transferred into FACS tubes (500 µL), and the different formulations were applied (1 µg mL^{-1}). After 30 min, samples were washed, and Fcγ receptors were blocked (see above). Then, spleen cells were incubated

with cell lineage characterizing antibodies specific for CD3 (labeled with eFl506), CD11b (SB600), CD11c (APC), CD19 (SB702), NK1.1 (PE), Ly6G (PE/eFl610) for 20 min at 4 °C. All antibodies were purchased from BioLegend (San Diego, CA) or Thermo Fisher. Samples were fixed and analyzed by flow cytometry (see above). The gating strategy is depicted in Figure S11, Supporting Information.

Animal Studies: Male C57BL/6 mice (Janvier Labs; body weight: 22.4 ± 1.7 g; age: 6–8 weeks) housed in the animal care facility of the University of Mainz were used in this study. The anesthetization of the animals was accomplished using an isoflurane vaporizer, where 2.5% of isoflurane was admixed with air. Anesthetized animals were injected with 5.29 ± 0.56 MBq of the respective radiolabeled compound in 100–150 µL of PBS via a tail vein (PET animals) or retroorbital (biodistribution animals). The applied masses for the nonassociated polyether lipids were <0.030 mg for [^{18}F]FTT-alkyne-BisHD-*hb*PG$_{63}$ and <0.88 mg for [^{18}F]FTT-trimannose-alkyne-BisHD-*hb*PG$_{63}$. For the corresponding liposomal formulations the applied masses were <0.055 mg for [^{18}F]FTT-alkyne-BisHD-*hb*PG$_{63}$ and <0.061 mg for [^{18}F]FTT-trimannose-alkyne-BisHD-*hb*PG$_{63}$. All experiments had previously been approved by the regional animal ethics committee and were conducted in accordance with the German Law for Animal Protection and the UKCCCR Guidelines.[23]

PET scans were run on a microPET Focus 120 (Siemens). For the dynamic PET scans of 1 h, data acquisition was started at the time of injection. For the 3.5–4 h static PET scans the mice were anesthetized for the injection, but were awake in the time span between injection and PET scan. During the PET scan the animals lay in a head first prone position. The list mode data files were reconstructed using a filtered backprojection reconstruction algorithm. The reconstruction was done using ASIPro 1.2. software. AMIDE software was utilized for image processing purposes. To accomplish the analysis of the PET data PMOD 3.6 software was used.

In order to assess the distribution of the radiolabeled compounds in different organs, injected animals ($n = 5$, per time point and per polyether lipid or liposome) were sacrificed after 1 or 4 h and organs of interest were collected. The tissue samples were weighed and the activity in the samples was measured in a γ-counter (2470 WIZARD^2 Automatic Gamma Counter, PerkinElmer).

Statistical Analysis: All statistical tests were performed using GraphPad 5 (GraphPad Software, San Diego, CA). Variances in data distribution were tested by one-way ANOVA, and statistical differences between groups were assessed by Tukey test (comparison > 2 groups) or unpaired Student´s *t*-test (2 groups). *p*-values below 0.05 were considered statistically significant.

Supporting Information

Supporting Information is available from the Wiley Online Library or from the author.

Acknowledgements

M.B. and M.K. contributed equally to this work. The authors thank Dr. Johannes Liermann for scientific support and helpful discussions regarding NMR spectroscopy of the investigated compounds. K.W. and M.W. are grateful to the Max-Planck Graduate Center (MPGC) as well as to the DFG in the context of the SFB 1066 for financial support. K.W., M.K., J.L., M.W., and M.S. are members of the graduate school of the SFB 1066.

Conflict of Interest

The authors declare no conflict of interest.

Keywords

DC-SIGN, dendritic cells, liposomes, targeting, trimannose

Received: October 2, 2019
Revised: January 18, 2020
Published online: March 1, 2020

[1] J. Banchereau, R. M. Steinman, *Nature* **1998**, *392*, 245.
[2] a) M. F. Lipscomb, B. J. Masten, *Physiol. Rev.* **2002**, *82*, 97; b) R. M. Steinman, J. Banchereau, *Nature* **2007**, *449*, 419.
[3] R. E. Berg, J. Forman, *Curr. Opin. Immunol.* **2006**, *18*, 338.
[4] R. V. Luckheeram, R. Zhou, A. D. Verma, B. Xia, *Clin. Dev. Immunol.* **2012**, *2012*, 925135.
[5] A. Makkouk, G. J. Weiner, *Cancer Res.* **2015**, *75*, 5.
[6] L. Shen, S. Krauthäuser, K. Fischer, D. Hobernik, Y. Abassi, A. Dzionek, A. Nikolaev, N. Voltz, M. Diken, M. Krummen, E. Montermann, I. Tubbe, S. Lorenz, D. Strand, H. Schild, S. Grabbe, M. Bros, *Nanomedicine* **2016**, *11*, 2647.
[7] U. Bulbake, S. Doppalapudi, N. Kommineni, W. Khan, *Pharmaceutics* **2017**, *9*, 12.
[8] A. Akbarzadeh, R. Rezaei-Sadabady, S. Davaran, S. W. Joo, N. Zarghami, Y. Hanifehpour, M. Samiei, M. Kouhi, K. Nejati-Koshki, *Nanoscale Res. Lett.* **2013**, *8*, 102.
[9] B. S. Pattni, V. V. Chupin, V. P. Torchilin, *Chem. Rev.* **2015**, *115*, 10938.
[10] a) C. G. Figdor, Y. van Kooyk, G. J. Adema, *Nat. Rev. Immunol.* **2002**, *2*, 77; b) A. Holla, A. Skerra, *Protein Eng., Des. Sel.* **2011**, *24*, 659.
[11] E. P. McGreal, J. L. Miller, S. Gordon, *Curr. Opin. Immunol.* **2005**, *17*, 18.
[12] E. J. Soilleux, L. S. Morris, G. Leslie, J. Chehimi, Q. Luo, E. Levroney, J. Trowsdale, L. J. Montaner, R. W. Doms, D. Weissman, *J. Leukocyte Biol.* **2002**, *71*, 445.
[13] J. M. Irache, H. H. Salman, C. Gamazo, S. Espuelas, *Expert Opin. Drug Delivery* **2008**, *5*, 703.
[14] D. A. Mitchell, A. J. Fadden, K. Drickamer, *J. Biol. Chem.* **2001**, *276*, 28939.
[15] H. Feinberg, D. A. Mitchell, K. Drickamer, W. I. Weis, *Science* **2001**, *294*, 2163.
[16] H. Feinberg, R. Castelli, K. Drickamer, P. H. Seeberger, W. I. Weis, *J. Biol. Chem.* **2007**, *282*, 4202.
[17] a) M. J. Copland, M. A. Baird, T. Rades, J. L. McKenzie, B. Becker, F. Reck, P. C. Tyler, N. M. Davies, *Vaccine* **2003**, *21*, 883; . b) K. L. White, T. Rades, R. H. Furneaux, P. C. Tyler, S. Hook, *J. Pharm. Pharmacol.* **2006**, *58*, 729.
[18] a) A. M. Hofmann, F. Wurm, E. Hühn, T. Nawroth, P. Langguth, H. Frey, *Biomacromolecules* **2010**, *11*, 568; . b) G. Kasza, G. Kali, A. Domján, L. Pethő, G. r. Szarka, B. Iván, *Macromolecules* **2017**, *50*, 3078.
[19] K. Wagener, M. Worm, S. Pektor, M. Schinnerer, R. Thiermann, M. Miederer, H. Frey, F. Rösch, *Biomacromolecules* **2018**, *19*, 2506.
[20] A. T. Reibel, S. S. Müller, S. Pektor, N. Bausbacher, M. Miederer, H. Frey, F. Rösch, *Biomacromolecules* **2015**, *16*, 842.
[21] M. Bé, V. Chisté, C. Dulieu, E. Browne, V. Chechev, N. Kuzmenko, R. Helmer, A. Nichols, E. Schönfeld, R. Dersch, Monograph, *Bureau International des Poids et Mesures, Sèvres, France* **2004**.
[22] a) I. Hellmuth, I. Freund, J. Schlöder, S. Seidu-Larry, K. Thüring, K. Slama, J. Langhanki, S. Kaloyanova, T. Eigenbrod, M. Krumb, *Front. Immunol.* **2017**, *8*, 312; b) S. Kramer, J. Langhanki, M. Krumb, T. Opatz, M. Bros, R. Zentel, *Macromol. Biosci.* **2019**, 1800481.
[23] P. Workman, E. Aboagye, F. Balkwill, A. Balmain, G. Bruder, D. Chaplin, J. Double, J. Everitt, D. Farningham, M. Glennie, *Br. J. Cancer* **2010**, *102*, 1555.